Second-order susceptibility imaging with polarization-resolved second harmonic generation microscopy

Second-order susceptibility imaging with polarization-resolved, second harmonic generation microscopy

Wei-Liang Chen[a], Tsung-Hsian Li [a], Ping-Jung Su[a], Chen-Kuan Chou[a], Peter Tramyeon Fwu[a], Sung-Jan Lin[b], Daekeun Kim[c], Peter T. C. So[c,d], and Chen-Yuan Dong[*a]
[a]Department of Physics, National Taiwan University, Taipei 106, Taiwan
[b]Department of Dermatology, National Taiwan University Hospital, Taipei 100, Taiwan
[c]Department of Mechanical Engineering, Massachusetts Institute of Technology, Cambridge, MA USA 02139
[d]Department of Biological Engineering, Massachusetts Institute of Technology, Cambridge, MA USA 02139

ABSTRACT

Second harmonic generation (SHG) microscopy has become an important tool for minimally invasive biomedical imaging. However, differentiation of different second harmonic generating species is mainly provided by morphological features. Using excitation polarization-resolved SHG microscopy we determined the ratios of the second-order susceptibility tensor elements at single pixel resolution. Mapping the resultant ratios for each pixel onto an image provides additional contrast for the differentiation of different sources of SHG. We demonstrate this technique by imaging collagen-muscle junction of chicken wing.

Keywords: Second harmonic generation, polarization, microscopy, collagen

1. INTRODUCTION

Second harmonic generation (SHG) microscopy has become an important imaging modality in biomedical optics [1-3]. Biological tissues such as muscles, tendons, skin dermis, and corneas are known strong generators of second harmonic signals [4-6]. SHG microscopy has been demonstrated to be an effective and minimally invasive imaging tool capable of probing a wide array of issues in biomedical studies including cell-extracellular matrix interaction, *in vivo* liver metabolism, cancer proliferation, cornea pathology, skin thermal effects, and tissue engineering [3-12]. In addition to morphological information, the excitation polarization dependences of SHG signal can provide structural information below the resolution of optical microscopy [4]. Furthermore, dependence of SHG signal on excitation polarization can be used to differentiate the tissues responsible for generating the second harmonic signals [4, 13-16]. Specifically, variations in the excitation polarization dependences of the SHG signal results from the difference in the second order susceptibility elements of the $\chi^{(2)}$ tensor. By acquiring polarization second harmonic images without sample rotation [17], χ tensor element ratios can be determined for each pixel of an SHG image. The resulting information can then be displayed as an image. Since different sources of SHG potentially have different susceptibility tensor elements, the contrast provided by such imaging allows possible differentiation of localized structural inhomogeneities that are difficult to differentiate by SHG intensity imaging alone. The differences in the χ tensor elements can potentially be used as a contrast mechanism not only for different second-harmonic generating molecules but also conformational changes in the molecule that produces the second harmonic signals. Possible application of this technique includes tissue engineering of cartilage where monitoring the type and distribution of the collagen produced is critical for determining the optimal conditions for cartilage production [12].

In this work, we obtained second order susceptibility (χ) tensor-resolved SHG images of the muscle tendon junction where the SHG polarization dependence has been studied previously. In this case, the SHG generators can be modeled as cylindrically symmetric coil molecules, where the number of independent χ tensor elements is significantly reduced [4, 13, 14]. Our approach involves using a discrete number of excitation polarization angles in producing χ tensor-resolved

[*] cydong@phys.ntu.edu.tw; phone +886-2-3366-5571; fax +886-2-33665244

Multiphoton Microscopy in the Biomedical Sciences X, edited by Ammasi Periasamy, Peter T. C. So, Karsten König, Proc. of SPIE Vol. 7569, 75691P · © 2010 SPIE · CCC code: 1605-7422/10/$18 · doi: 10.1117/12.843015

SHG images. The potential of this technique for *in vivo* applications led us to perform our work in an epi-illuminated SHG microscope, despite the increased complexity of interpreting backward SHG signals [18, 19].

2. MATERIAL AND METHODS

2.1 Second harmonic generation microscope

Figure 1 shows a schematic diagram of the epi-illuminated polarization SHG microscope used in our experiment. The excitation source is a pulsed femtosecond laser (Tsunami, Spectral Physics, Mountain View, CA) tuned to 780 nm. The power of the excitation is controlled by a half-wave plate (HWP) and a linear polarizer while the polarization property is controlled by an additional half-wave plate (HWP2) and a quarter-wave plate (QWP). The excitation beam passes through our custom built scanning system and enters the microscope. The beam is reflected onto the sample by the short pass, main dichroic mirror (700dcspxruv-2p, Chroma Technology, Rockingham, VT). The SHG signal from the sample is collected in the backward direction and is selected by the combination of a dichroic mirror and a narrow band pass filter (435DCXR and HQ390/22m-2p, Chroma technology). The signal is detected in single photon counting mode using a photomultiplier tube (R7400P, Hamamatsu, Japan), and a custom built discriminator. A computer coordinates the scanning control and the signal detection to form the final image.

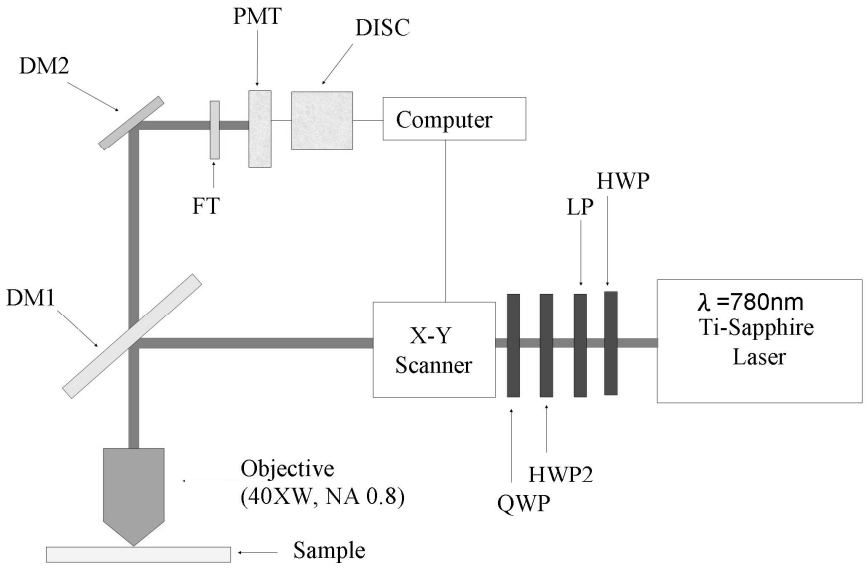

Figure 1. Diagram of experimental setup for the polarization resolved second harmonic generation microscope: HWP, half-wave plate; LP, linear polarizer; HWP2, half-wave plate; QWP, quarter-wave plate; DM1, main dichroic mirror; DM2, dichroic mirror; FT, narrow band pass filter; PMT, photomultiplier tube; DISC, discriminator.

2.2 Chi tensor determination

To obtain SHG polarization information, we incident the sample with linearly polarized excitation oriented at different polarization angles. This was achieved by rotating HWP2 and QWP to compensate for the depolarization effect of the main dichroic mirror [17]. By varying the combination of HWP2 and QWP angles, we acquired SHG images of the sample using excitation with arbitrary polarization angle θ. The data collected for a particular field of view consists of a stack of images with a linearly polarized excitation oriented along various angle,θ. The ability to acquire SHG images without sample rotation allows us to obtain with ease, the pixel-resolved, tensor SHG polarization images.

To determine the ratios of the second order susceptibility tensor elements, we assume the molecules responsible for the second harmonic generation are bundled and well aligned within the size of our point spread function. This assumption allows us to approximate the susceptibility tensor to be cylindrically symmetric, which reduces the number of independent χ tensor elements to four [4]. In our experimental setup, the laser is incident along the +y direction, and the sample lies in the x-z plane with the axis of symmetry along the z' direction. Under such configuration and coordinate system, we can write the total second harmonic generation signal intensity, I_{SHG} as [4, 13]

$$I_{SHG} \propto E^4 \left\{ (\chi_{zxx} \sin^2\theta + \chi_{zzz} \cos^2\theta)^2 + \chi_{xzx}^2 \sin^2(2\theta) \right\}, \quad (1)$$

where χ_{zxx}, χ_{zzz}, and χ_{xzx} are independent second order susceptibility tensor elements, E is the amplitude of the incident electric field, and θ, is the laser polarization angle measured with respect to the fiber z' axis. Although we assume the molecules are aligned within a point spread function, the fiber orientation within an image can change. For a fixed laser polarization angle θ_e, the angle between the fiber direction θ_o and the laser polarization angle can change. The angle θ can be expressed as $\theta = \theta_e - \theta_o$ where θ_e and θ_o are measured with respect to the fixed z-axis in the plane of the sample. Since we only measure the relative change in the SHG intensity as a function of the incident laser polarization angle, we can introduce an overall multiplication factor, c, and rewrite Eq. (1) as

$$I_{SHG} = c \cdot \{ [\sin^2(\theta_e - \theta_\circ) + (\chi_{zzz} / \chi_{zxx}) \cos^2(\theta_e - \theta_\circ)]^2 + (\chi_{xzx} / \chi_{zxx})^2 \sin^2(2(\theta_e - \theta_\circ)) \}. \quad (2)$$

We experimentally measure the SHG intensity I_{SHG} at 21 different excitation polarization angle, θ_e, and used Eq. (2) to determine the values of c, the fiber angle θ_o, and the ratios of the tensor elements χ_{zzz}/χ_{zxx}, and χ_{xzx}/χ_{zxx} that gives the best fit to the experimental data. The use of 21 different polarization angles allows for a more accurate determination of the fitting parameters given the large intrinsic fluctuations of the SHG signal in an epi-illuminated configuration. Since this model fitting is done on each individual pixel of the acquired polarization resolved SHG images, the values of each tensor element ratio can be represented as an image. The variation in the χ tensor elements therefore provides a contrast mechanism for differentiating different sources of SHG.

3. RESULTS

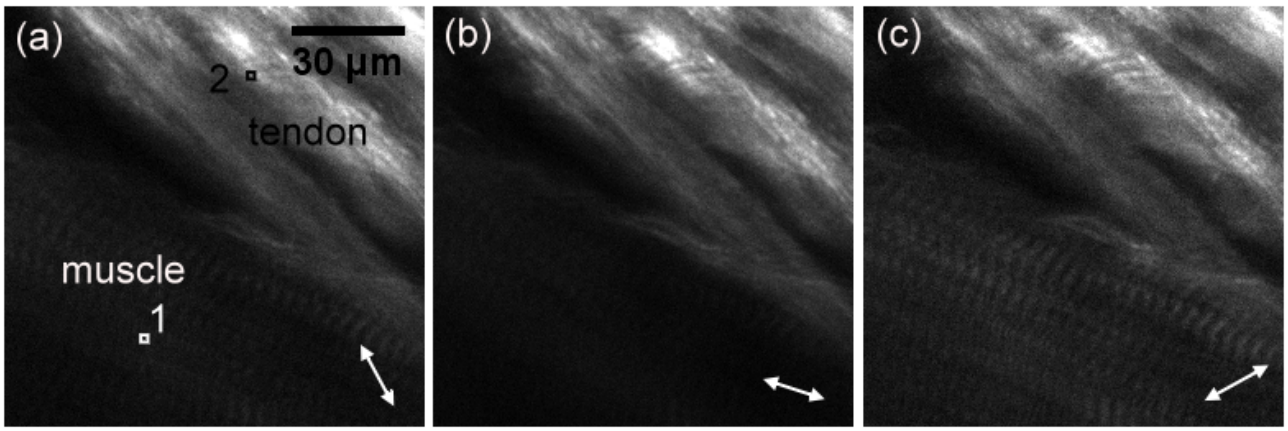

Fig. 2 SHG image of tendon-muscle junction of chicken wing with different incident laser polarization. The arrow in the lower right hand corner shows the direction of laser polarization.

To demonstrate this technique, we imaged the tendon-muscle junction of a chicken wing. Since polarization dependence of SHG from both tendon and muscle has been well studied[4, 13, 14, 20], the tendon-muscle junction is a good candidate for the testing of our method. Figure 2 shows four images of the junction with different excitation polarization. The arrow on the lower right hand side of each image shows the direction of the polarization of the incident laser.

Intensity variations in the SHG images are visible as the incident laser polarization changes. Shown on the upper right of the image is the fiber pattern found in typical SHG images of tendon. On the other hand, the lower left side of the image shows the pattern that is found in SHG muscle imaging[4, 13, 14, 21]. The contrast between the muscle and the tendon in the SHG image is provided by the difference in the SHG intensity from the two sources and the difference in their morphology. In Fig. 2 although the tendon and the muscle fiber direction are similar, the SHG from tendon is brightest when the incident laser polarization is approximately parallel to the fiber (Fig. 2 (b)), while the SHG from the muscle is the brightest when the polarization is at an angle of approximately 45° from the muscle fiber (Fig. 2(c)).

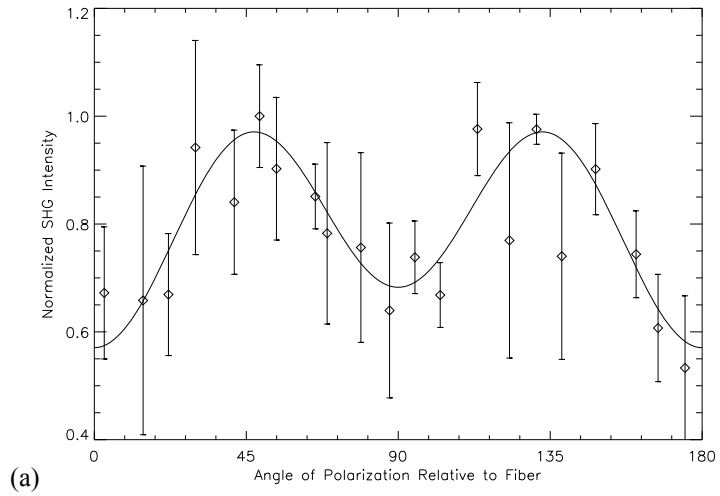

(a)

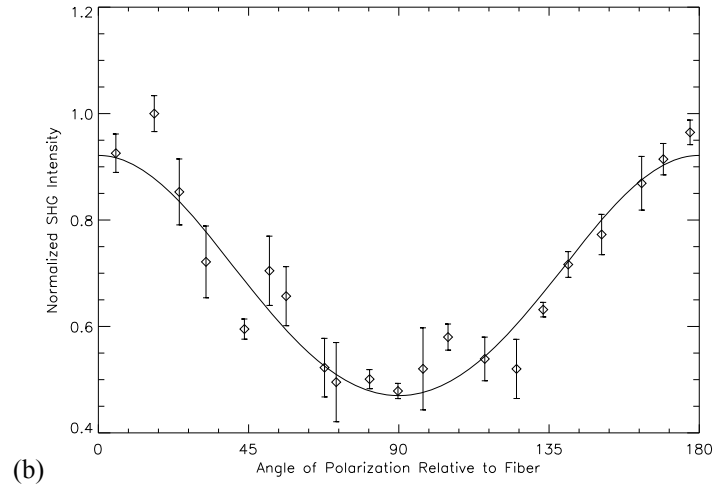

(b)

Fig. 3 Plot of the polarization dependence of SHG intensity on the incident laser polarization angle for the two marked points in Fig. 2. (a) and (b) corresponds to the location 1 and 2 respectively. The curve is the model fitting to the data points. For (a), the χ ratios are $\chi_{zzz}/\chi_{zxx} = 1.4$ and $\chi_{xzx}/\chi_{zxx} = 0$. For (b), the χ ratios are $\chi_{zzz}/\chi_{zxx} = 0.91$ and $\chi_{xzx}/\chi_{zxx} = 0.71$.

We can quantify the incident polarization dependence by plotting the SHG intensity variation with incident polarization angle. Figure 3 (a) and (b) show respectively the plot of intensity dependence on the polarization for pixel locations 1 and 2 in Figure 2 (a). The error bars are the standard deviation over three repeated image acquisition. The curve in each of the plots is the model fit to the data points using Eq. (2). By performing the model fit for each individual pixel, we can display the results of the fitted model parameters as an image. Figure 4 (b) shows the model fitted fiber angle for the SHG image shown in Figure 4(a). Similarly, the susceptibility tensor imaging is shown in Figure 4 (c) and (d) for the ratios χ_{zzz}/χ_{zxx} and χ_{xzx}/χ_{zxx} of the tendon-muscle junction. We used the brightness to represent the fiber angles and for the values of the ratios. The corresponding values for the different brightness is shown in the calibration bar on the upper right of the images.

As can be seen from Fig. 4(c), the ratio (χ_{zzz}/χ_{zxx}) is effective in contrasting the area of SHG that we know through morphology to be from the tendon and from the muscle. The χ_{xzx}/χ_{zxx} ratio imaging, however, is not as effective in showing such contrast. If we inspect Eq. (2) more closely, we see that the χ_{xzx}/χ_{zxx} term appear as the coefficient of the term $\sin^2(2(\theta_e - \theta_\circ))$, which is more sensitive to the smaller variations in the SHG intensity change with polarization angle.

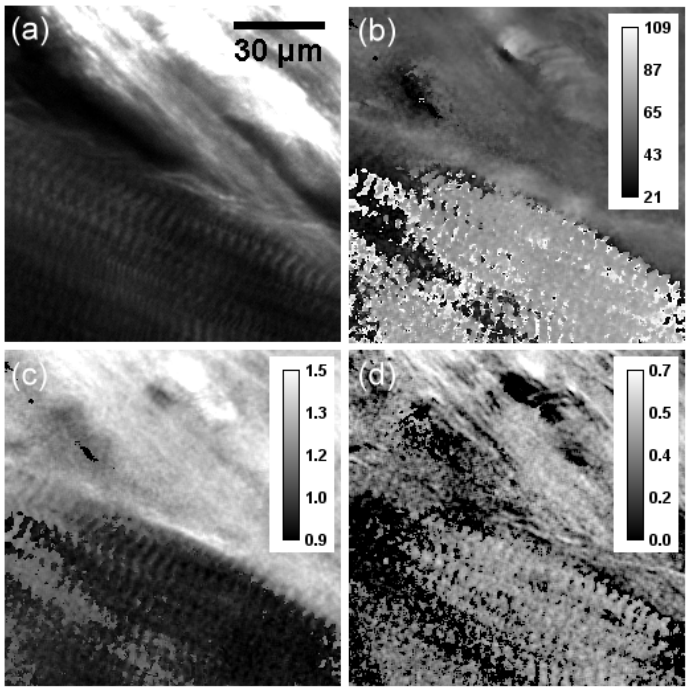

Fig. 4 (a) SHG image of muscle-tendon junction. (b) fiber angle, and (c), (d) χ tensor ratio (χ_{xzx}/χ_{zxx}), (χ_{zzz}/χ_{zxx}) displayed as an image for the tendon-muscle junction shown in (a). The corresponding calibration bar is shown in the upper right hand corners of the images.

The histogram distribution of the χ_{zzz}/χ_{zxx} image (Fig. 4(d)) of muscle-tendon junction is shown in Figure 5. The curve is a fit assuming the distribution is a sum of two Gaussian functions with centers at 1.3±0.1 and 0.92±0.04. The errors are one standard deviation of the fitted Gaussian profile. The first peak at 1.3 corresponds to the susceptibility ratio χ_{zzz}/χ_{zxx} for tendon, is consistent with previous findings, while the second peak of 0.92 due to the muscle fiber is smaller than previous findings [4]. This may be due structural differences of muscle at the collagen-muscle junction.

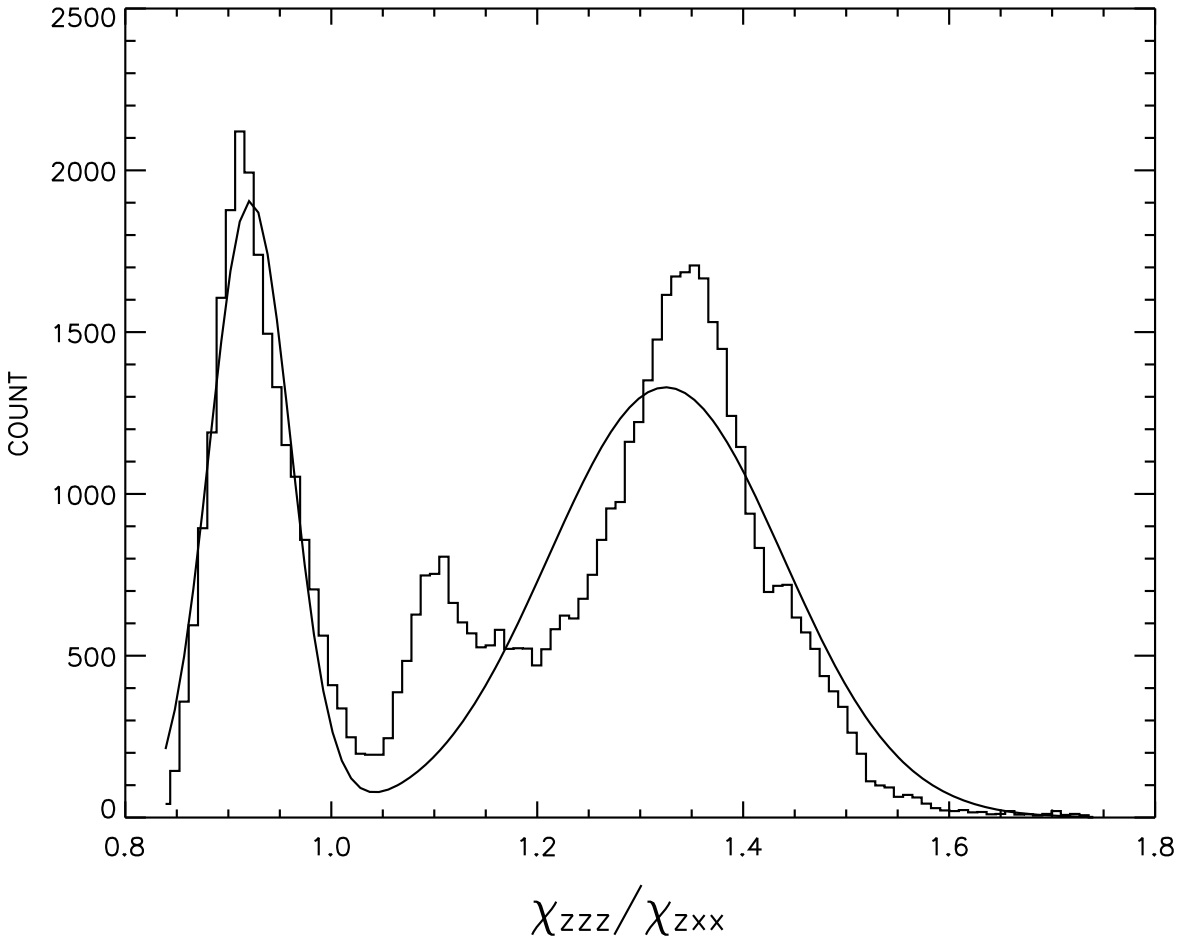

Fig. 5 Histogram plot of muscle-tendon junction χ_{zzz}/χ_{zxx} imaging. The line shows the fitting of the histogram using a sum of two Gaussian function.

4. CONCLUSION

By measuring the dependence of SHG intensity on the incident laser polarization without sample rotation, we can determine the χ tensor element ratios χ_{zzz}/χ_{zxx} and χ_{xzx}/χ_{zxx} to single pixel resolution. The results can be displayed as an image and used to distinguish the position of different sources of SHG signal. We applied this susceptibility tensor microscopy technique to the tendon-muscle junction of chicken wing, and found that the ratio χ_{zzz}/χ_{zxx} can be used to effectively separate different sources of SHG in an SHG image. Since our experiment was performed on an epi-illuminated microscope configuration, this approach can potentially be applied to *in vivo* studies to differentiate molecular species responsible for generating second harmonic signals.

.

REFERENCES

1. Campagnola, P. J. and Loew, L. M., "Second-harmonic imaging microscopy for visualizing biomolecular arrays in cells, tissues and organisms," Nature Biotechnology 21(11), 1356-1360 (2003)

2. Zipfel, W. R., Williams, R. M., Christie, R., Nikitin, A. Y., Hyman, B. T. and Webb, W. W., "Live tissue intrinsic emission microscopy using multiphoton-excited native fluorescence and second harmonic generation," Proceedings of the National Academy of Sciences of the United States of America 100(12), 7075-7080 (2003)
3. Zoumi, A., Yeh, A. and Tromberg, B. J., "Imaging cells and extracellular matrix in vivo by using second-harmonic generation and two-photon excited fluorescence," Proceedings of the National Academy of Sciences of the United States of America 99(17), 11014-11019 (2002)
4. Plotnikov, S. V., Millard, A. C., Campagnola, P. J. and Mohler, W. A., "Characterization of the Myosin-Based Source for Second-Harmonic Generation from Muscle Sarcomeres," Biophysical Journal 90(2), 693-703 (2006)
5. Teng, S. W., Tan, H. Y., Peng, J. L., Lin, H. H., Kim, K. H., Lo, W., Sun, Y., Lin, W. C., Lin, S. J., Jee, S. H., So, P. T. C. and Dong, C. Y., "Multiphoton autofluorescence and second-harmonic generation imaging of the ex vivo porcine eye," Investigative Ophthalmology & Visual Science 47(3), 1216-1224 (2006)
6. Campagnola, P. J., Millard, A. C., Terasaki, M., Hoppe, P. E., Malone, C. J. and Mohler, W. A., "Three-dimensional high-resolution second-harmonic generation imaging of endogenous structural proteins in biological tissues," Biophysical Journal 82(1), 493-508 (2002)
7. Liu, Y., Chen, H. C., Yang, S. M., Sun, T. L., Lo, W., Chiou, L. L., Huang, G. T., Dong, C. Y. and Lee, H. S., "Visualization of hepatobiliary excretory function by intravital multiphoton microscopy," Journal of Biomedical Optics 12(1), - (2007)
8. Brown, E. B., Campbell, R. B., Tsuzuki, Y., Xu, L., Carmeliet, P., Fukumura, D. and Jain, R. K., "In vivo measurement of gene expression, angiogenesis and physiological function in tumors using multiphoton laser scanning microscopy," Nature Medicine 7(7), 864-868 (2001)
9. Tan, H. Y., Sun, Y., Lo, W., Lin, S. J., Hsiao, C. H., Chen, Y. F., Huang, S. C. M., Lin, W. C., Jee, S. H., Yu, H. S. and Dong, C. Y., "Multiphoton fluorescence and second harmonic generation imaging of the structural alterations in keratoconus ex vivo," Investigative Ophthalmology & Visual Science 47(12), 5251-5259 (2006)
10. Lin, S. J., Jee, S. H., Kuo, C. J., Wu, R. J., Lin, W. C., Chen, J. S., Liao, Y. H., Hsu, C. J., Tsai, T. F., Chen, Y. F. and Dong, C. Y., "Discrimination of basal cell carcinoma from normal dermal stroma by quantitative multiphoton imaging," Opt Lett 31(18), 2756-2758 (2006)
11. Lin, M. G., Yang, T. L., Chiang, C. T., Kao, H. C., Lee, J. N., Lo, W., Jee, S. H., Chen, Y. F., Dong, C. Y. and Lin, S. J., "Evaluation of dermal thermal damage by multiphoton autofluorescence and second-harmonic-generation microscopy," Journal of Biomedical Optics 11(6), - (2006)
12. Lee, H. S., Teng, S. W., Chen, H. C., Lo, W., Sun, Y., Lin, T. Y., Chiou, L. L., Jiang, C. C. and Dong, C. Y., "Imaging human bone marrow stem cell morphogenesis in polyglycolic acid scaffold by multiphoton microscopy," Tissue Engineering 12(10), 2835-2841 (2006)
13. Chu, S. W., Chen, S. Y., Chern, G. W., Tsai, T. H., Chen, Y. C., Lin, B. L. and Sun, C. K., "Studies of x((2))/x((3)) tensors in submicron-scaled bio-tissues by polarization harmonics optical microscopy," Biophysical Journal 86(6), 3914-3922 (2004)
14. Stoller, P., Kim, B. M., Rubenchik, A. M., Reiser, K. M. and Da Silva, L. B., "Polarization-dependent optical second-harmonic imaging of a rat-tail tendon," Journal of Biomedical Optics 7(2), 205-214 (2002)
15. Cox, G., Xu, P., Sheppard, C., Ramshaw, J. and Unit, E. M., "Characterization of the Second Harmonic Signal from Collagen," Proc. of SPIE Vol 4963(33 (2003)
16. Chu, S. W., Tai, S. P., Sun, C. K. and Lin, C. H., "Selective imaging in second-harmonic-generation microscopy by polarization manipulation," Applied Physics Letters 91(103903 (2007)
17. Chou, C. K., Chen, W. L., Fwu, P. T., Lin, S. J., Lee, H. S. and Dong, C. Y., "Polarization ellipticity compensation in polarization second-harmonic generation microscopy without specimen rotation," Journal of Biomedical Optics 13(1), - (2008)
18. Nadiarnykh, O., LaComb, R., Campagnola, P. J. and Mohler, W. A., "Coherent and incoherent SHG in fibrillar cellulose matrices," Opt Express 15(6), 3348-3360 (2007)
19. LaComb, R., Nadiarnykh, O., Townsend, S. S. and Campagnola, P. J., "Phase matching considerations in second harmonic generation from tissues: Effects on emission directionality, conversion efficiency and observed morphology," Optics Communications 281(7), 1823-1832 (2008)
20. Stoller, P., Reiser, K. M., Celliers, P. M. and Rubenchik, A. M., "Polarization-Modulated Second Harmonic Generation in Collagen," Biophysical Journal 82(6), 3330-3342 (2002)
21. Williams, R. M., Zipfel, W. R. and Webb, W. W., "Interpreting second-harmonic generation images of collagen I fibrils," Biophysical Journal 88(2), 1377-1386 (2005)